arXiv:1405.7861v1 [physics.optics] 30 May 2014

Manipulating the Interaction between Localized and Delocalized Surface Plasmon Polaritons in Graphene

Renwen Yu,[1] Rasoul Alaee,[2] Falk Lederer,[1] and Carsten Rockstuhl[2,3]

[1]*Institute of Condensed Matter Theory and Solid State Optics, Abbe Center of Photonics, Friedrich-Schiller-Universität Jena, D-07743 Jena, Germany*
[2]*Institute of Theoretical Solid State Physics, Karlsruhe Institute of Technology, Wolfgang-Gaede-Strasse 1, 76131 Karlsruhe, Germany*
[3]*Institute of Nanotechnology, Karlsruhe Institute of Technology, P.O. Box 3640, 76021 Karlsruhe, Germany*

The excitation of localized or delocalized surface plasmon polaritons in nanostructured or extended graphene has attracted a steadily increasing attention due to their promising applications in sensors, switches, and filters. These single resonances may couple and intriguing spectral signatures can be achieved by exploiting the entailing hybridization. Whereas thus far only the coupling between localized *or* delocalized surface plasmon polaritons has been studied in graphene nanostructures, we consider here the interaction between a localized *and* a delocalized surface plasmon polariton. This interaction can be achieved by two different schemes that reside on either evanescent near-field coupling or far-field interference. All observable phenomena are corroborated by analytical considerations, providing insight into the physics and paving the way for compact and tunable optical components at infrared and terahertz frequencies.

PACS numbers: 78.67.Wj, 78.20.-e, 73.21.-b, 71.70.Gm

I. INTRODUCTION

Graphene, a two-dimensional (2D) arrangement of carbon atoms, enables a multitude of exciting applications due to its extraordinary electrical, mechanical, but especially, optical properties [1–6]. The most prominent optical peculiarity is likely its non-dispersive (in a broad spectral domain) absorption of about 2.3% of an incident electromagnetic wave [7]. This might sound marginal but is actually exceptionally large, considering that a monolayer of a material with negligible thickness is responsible for such observation.

But this absorption can be even considerably enlarged in a narrow frequency range. This is possible by exploiting either delocalized (DSPPs) or localized surface plasmon polaritons (LSPPs). There, the electromagnetic field is resonantly coupled to oscillations of the surface charge density leading to a strong enhancement of light-matter-interaction at the nanoscale [8]. The excitation of either graphene DSPPs or LSPPs at IR and THz frequencies has been already demonstrated while relying on various graphene micro- or nanostructures [9–15]. They have been employed to achieve novel exciting functionalities, such as perfect absorbers [16–18], broadband polarizers [19, 20], THz reflectarrays [21], tunable THz cloaking [22, 23], or tunable graphene antennas [24].

However, not just individual resonances sustained by micro- or nanostructured graphene have been studied, but also the excitation of multiples thereof. This can be either done with suitably designed individual elements that exhibit multiple resonances or while coupling multiple elements with single resonances. Effects like plasmon hybridization [25] or spectral interference give rise to involved but intriguing spectral signatures. They are extremely appealing for a larger variety of applications such as plasmon-induced transparency (PIT) [26, 27], tunable Fano resonance sensing [28], and strong mode confinement [29, 30].

Recently, PIT has also been demonstrated in periodically patterned graphene nanostrips. This was possible by exploiting the spectral interference between a bright and a dark LSPP mode sustained by periodically patterned graphene nanostrips [31]. Alternatively, a double graphene layer structure acting as a plasmonic waveguide switch has been proposed that exploits the culling between two DSPP modes supported by those two graphene layers [32].

However, thus far only the coupling between graphene DSPPs or LSPPs has been considered, but never that between a DSPP and a LSPP. With the purpose to understand the observable phenomena in such regime, we study here comprehensively this important phenomenon. Emphasis is put on the exploration of two different schemes where interaction relies either on near-field coupling or far-field interference.

The first scheme exploits a graphene-only device where a LSPP, supported by a periodic array of graphene ribbons (PAGR), and a DSPP, supported by an extended graphene layer, are coupled. This coupling is evoked by the near-field overlap of both SPPs if the PAGR and the graphene layer are very close to each other. The strength of the coupling can get very large by carefully tuning the geometrical parameters of the system. Consequently, the formation of hybrid DSPP-LSPP polaritons can be witnessed.

The second scheme allows to study the interference between LSPPs and DSPPs in a far-field interaction regime, facilitated by a dielectric diffractive grating below the

bottom graphene layer. In this regime, a pronounced Fabry-Perot (FP) effect needs to be taken into account. A simple picture considering the entire structure as an effective FP cavity is proposed to provide an intuitive understanding of the far-field interference phenomenon. The numerical results for both interaction schemes are corroborated by analytical models. They yield clear insights into the intriguing optical phenomena observed.

II. NEAR-FIELD COUPLING SCHEME (NFCS)

A schematic view of the proposed near-field coupling scheme (NFCS) is displayed in Fig. 1. The entire structure is assumed to be imbedded in an ambient material with a relative permittivity of $\varepsilon = 2.25$. This, however, is by no means a limitation and any other dielectric material environment could have been considered as well. The PAGR on top (array period P, ribbon width W) and the bottom graphene layer are separated by a dielectric spacer of thickness d. Throughout this work, we assume that the polaritons are excited by a normally incident TM-polarized wave propagating in negative y direction with magnetic field polarized along z direction. Then, the optical response of the PAGR is characterized by the LSPP resonance [13, 33]. Moreover, simultaneously, its periodicity leads to the excitation of the DSPP modes in the nearby graphene layer due to Bragg diffraction [12, 34]. Due to the evanescent coupling the excitation efficiency of the DSPP modes in the bottom graphene layer depends strongly on the separation distance d to the PAGR [12], as we will show in the following. The surface conductivity of graphene is modelled within the local random phase approximation including the finite temperature correction as [8]

$$\sigma(\omega) = \frac{e^2 E_\mathrm{F}}{\pi\hbar^2}\frac{i}{\omega + i\tau^{-1}}. \tag{1}$$

Here, E_F is the Fermi energy, $\tau = \mu E_\mathrm{F}/(e v_\mathrm{F}^2)$ is the relaxation time, $\hbar$ is the reduced Planck constant, e is the electron charge, $v_\mathrm{F} \approx 10^6\,\mathrm{m/s}$ is the Fermi velocity, and $\mu \approx 10000\,\mathrm{cm^2/V\cdot s}$ is the impurity-limited DC mobility [1]. All numerical simulations were performed by using a finite element method (FEM) based solver for Maxwell's equations (*COMSOL Multiphysics*).

To start the analysis a grating period $P = 600\,\mathrm{nm}$ has been chosen. The Fermi energy level $E_\mathrm{F} = 600\,\mathrm{meV}$ is the same in the upper PAGR and the bottom graphene layer. The simulated absorption spectra are shown in Figs. 2(a) and (b) for two different ribbon widths W as a function of the spacer thickness in the interval from $d = 50\,\mathrm{nm}$ to $d = 350\,\mathrm{nm}$. The white dashed and dash-doted lines indicate the spectral positions of the DSPPs of the isolated graphene layer excited by the first and second Bragg diffraction order, respectively. They are calculated from the following equation [12, 14]

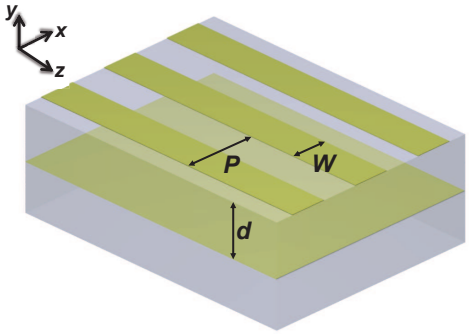

Fig. 1: Schematic view of the near-field coupling scheme. The PAGR (array period P and ribbon width W) and the bottom graphene layer are separated by a dielectric spacer of thickness d.

$$\omega_\mathrm{D} = \sqrt{\frac{2Ne^2 E_\mathrm{F}}{\hbar^2\varepsilon_0(\varepsilon_1+\varepsilon_2)P}}, \tag{2}$$

where ε_0 is the vacuum permittivity, ε_1 and ε_2 are the permittivities of the materials above and below the graphene layer, and N is an integer denoting the Bragg diffraction order. The spectral position of the bare LSPP mode, indicated by the white solid line, is numerically calculated from one isolated PAGR with identical Fermi energy and geometrical parameters.

In Fig. 2(a), for $W = 150\,\mathrm{nm}$ and for a large spacer thickness of $d = 350\,\mathrm{nm}$, only a single but strong absorption peak emerges at around 25.6 THz. This absorption peak is related to the LSPP resonance, indicated by the white solid line. The mode shape is depicted in Fig. 2(c) and changes only slightly when d decreases down to 100 nm.

When the separation distance decreases to about $d = 220\,\mathrm{nm}$, another smaller absorption peak emerges at around 21.5 THz. It is associated with the first Bragg diffraction order ($N = 1$) and constitutes a hybrid DSPP-LSPP resonance emerging from the bare DSPP mode supported by the graphene layer. The redshift of this hybrid mode and the blueshift of the LSPP resonance with decreasing d arises from the enhanced mutual near-field interaction and is a signature of the small but notable hybridization.

When the separation distance is further decreased to about $d = 120\,\mathrm{nm}$, a third absorption peak appears at higher frequency (around 30.5 THz). It is related to another hybrid DSSP-LSSP mode branching off the second order ($N = 2$) DSPP resonance. The gradual appearance of the hybrid modes essentially supported by the bottom graphene layer is due to the increasing excitation efficiency through the upper PAGR when the spacer

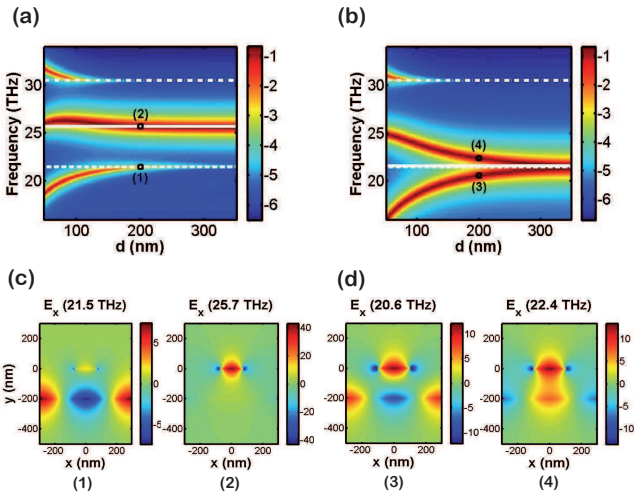

Fig. 2: (a) and (b): Simulated absorption spectra for two different ribbon widths: (a) $W = 150\,\mathrm{nm}$; (b) $W = 210\,\mathrm{nm}$. The spectral positions of the bare modes are indicated by white horizontal lines (solid line: LSPP mode, dashed line: first order DSPP mode, dashed-dotted line: second order DSPP mode). The spectra are plotted in a logarithmic scale. (c) and (d): Electric field distribution E_x of the absorption peaks corresponding to the positions indicated by (1), (2), (3) and (4) in panels (a) and (b), respectively. Note that the upper PAGR and the graphene layer are located at $y = 0$ and $y = -200\,\mathrm{nm}$, respectively. All local electric field distributions are normalized to the incident field.

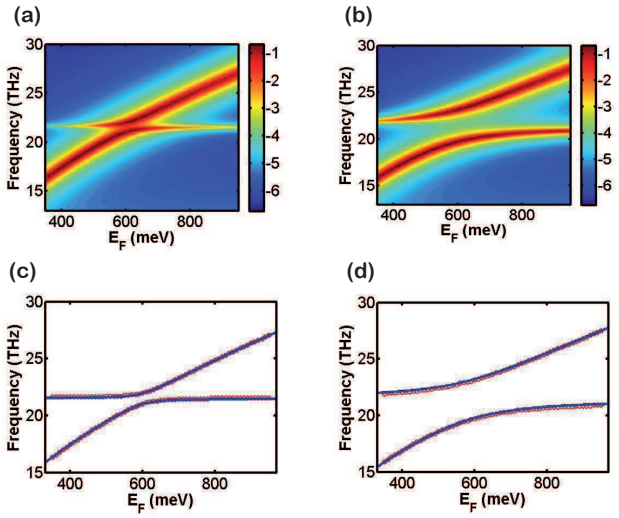

Fig. 3: (a) and (b): Simulated absorption spectra as function of the Fermi energy at two different separation distances: (a) $d = 260\,\mathrm{nm}$; (b) $d = 140\,\mathrm{nm}$. The spectra are plotted in a logarithmic scale. (c) and (d): Positions of the absorption peaks (red circles) extracted from panels (a) and (b) as a function of the Fermi energy E_F. The blue solid curves represent the analytical results from Eq. 4.

thickness d decreases because of the larger modal overlap between the LSPP and the DSPP. The higher the diffraction order from the PAGR that is used to excite the DSPP, the shorter is the decay length of the associated evanescent wave. Therefore a notably amplitude necessary for the excitation only exists below a specific spacer thickness, and this distance gets smaller the larger the diffraction order is. At the smallest considered spacer thickness of $d = 50\,\mathrm{nm}$, a large enhancement of the resonance strength of the DSPP-originated hybrid mode resonances at 18.7 THz and 31.7 THz can be recognized. This indicates a strong near field coupling and energy exchange between the LSPP and DSPP modes in graphene. Moreover, after interacting with the second order DSPP mode, the LSPP mode slightly redshifts, accompanied by a blueshift of the second order DSPP mode.

More dramatic variations of the optical response can be recognized in Fig. 2(b). There, the ribbon width was slightly increased to $W = 210\,\mathrm{nm}$ to achieve a spectral coincidence of the bare LSPP mode with the bare first order DSPP mode at about 21.5 THz. As a result a bonding [Fig. 2(d4)] and an anti-bonding [Fig. 2(d3)] hybrid DSPP-LSPP mode occur at smaller spacer thicknesses d. When increasing d, those two polariton modes degenerate.

In order to show that the coupling strength gets enhanced when the spectral positions of the LSPP mode (ω_L) and the first order DSPP mode (ω_D) coincide, the electric field distributions at a fixed separation distance $d = 200\,\mathrm{nm}$ are depicted in Figs. 2(c) and (d). It can be seen that when $\omega_\mathrm{L} \neq \omega_\mathrm{D}$, the electric field is mainly either concentrated in the bottom graphene layer or in the upper PAGR, as shown in Fig. 2(c). The field distributions of these weakly hybrid modes resemble either the bare LSPP mode or the bare first order DSPP mode [12]. However, when $\omega_\mathrm{L} \approx \omega_\mathrm{D}$, the electric field is concentrated in both upper PAGR and bottom graphene layer as shown in Fig. 2(d). This indicates an enhanced mode mixing and a larger coupling strength, and also demonstrates the formation of genuine bonding and anti-bonding LSPP-DSPP polaritons. In addition to varying the ribbon width W as we have shown in Fig. 2, the coupling between the LSPP mode and the second order DSPP mode can also be controlled by properly adjusting the array period P.

The Fermi energy of graphene can be dynamically tuned by electrical gating or chemical doping [1]. Thus, a similar tunability can also be expected due to the dynamical manipulation of the coupling between the LSPP and DSPP modes. Here, we assume that the geometric parameters of the upper PAGR are fixed as $W = 210\,\mathrm{nm}$ and $P = 600\,\mathrm{nm}$. The Fermi energy $E_\mathrm{F} = 600\,\mathrm{meV}$ is constant in the bottom graphene layer, but is subject to changes in the upper PAGR to investigate the tunability inside our NFCS.

As already shown in Fig. 2 the coupling between the DSPP and the LSPP modes can strongly enhance the

DSPP resonance. Thus, the energy exchange between the LSPP and DSPP modes is enhanced as well, given that the DSPP mode and the LSPP mode coincide spectrally. This leads to a splitting of the absorption peak at the spectral position of the DSPP mode, which is fixed in this case. Moreover, we observe that the coupling strength can be modified by tuning the Fermi energy E_{F} of the upper PAGR. The variation of the induced polariton modes with different Fermi energy is displayed in Fig. 3. Simulated absorption spectra with two different separation distances d are displayed in Figs. 3(a) and (b). It can be see that as E_{F} is varied, an obvious anticrossing feature is observed in both Figs. 3(a) and (b). At smaller E_{F}, the lower polariton behaves LSPP-like with a broad spectral width. When E_{F} is tuned towards the DSPP mode, this polariton mode changes its nature and gradually DSPP-like features emerge such as with narrow spectral width. The upper polariton mode follows the opposite route.

In Figs. 3(c) and (d), the spectral positions of the absorption maxima extracted from Figs. 3(a) and (b) are depicted as red circles, which indicate the induced upper and lower LSPP-DSPP polariton modes (ω_{u} and ω_{l}). At a Fermi energy $E_{\mathrm{F}} = 600\,\mathrm{meV}$, the two polariton modes anticross. The Rabi splitting $2\hbar\omega_\delta$ is 3.9 meV and 14.3 meV for the cases of the two separation distance $d = 260\,\mathrm{nm}$ and $d = 140\,\mathrm{nm}$, respectively. This indicates the coupling strength of the LSPP-DSPP interaction in a sense that the Rabi splitting becomes larger with decreasing the separation distance d since the interaction between the LSPP and DSPP modes is stronger. The blue solid curves are the results of solving the eigenvalue problem

$$\hat{H}\Psi = \hbar\omega_{\mathrm{u,l}}\Psi, \tag{3}$$

with eigenvector Ψ and interaction Hamiltonian $\hat{H} = \hbar\begin{pmatrix} \omega_{\mathrm{D}} & \omega_\delta \\ \omega_\delta & \omega_{\mathrm{L}}(E_{\mathrm{F}}) \end{pmatrix}$. Here, the eigenenergy of the DSPP mode is $\hbar\omega_{\mathrm{D}} = 88.9\,\mathrm{meV}$ and is derived from the spectral position of the bare DSPP mode, as shown in Fig. 2(b). The eigenfrequency of the bare LSPP mode, $\omega_{\mathrm{L}}(E_{\mathrm{F}})$, can be derived from fitting the simulation result to the relation $\omega_{\mathrm{L}} \propto \sqrt{E_{\mathrm{F}}}$ [13, 35]. Eventually, the eigenfrequency of the induced polariton modes is found as [36, 37]

$$\omega_{\mathrm{u,l}}(E_{\mathrm{F}}) = \frac{\omega_{\mathrm{L}}(E_{\mathrm{F}}) + \omega_{\mathrm{D}}}{2} \pm \sqrt{\omega_\delta^2 + \frac{\left[\omega_{\mathrm{L}}(E_{\mathrm{F}}) - \omega_{\mathrm{D}}\right]^2}{4}}. \tag{4}$$

The analytical results,depicted in Figs. 3(c) and (d) as blue solid curves, are in excellent agreement with the simulated ones.

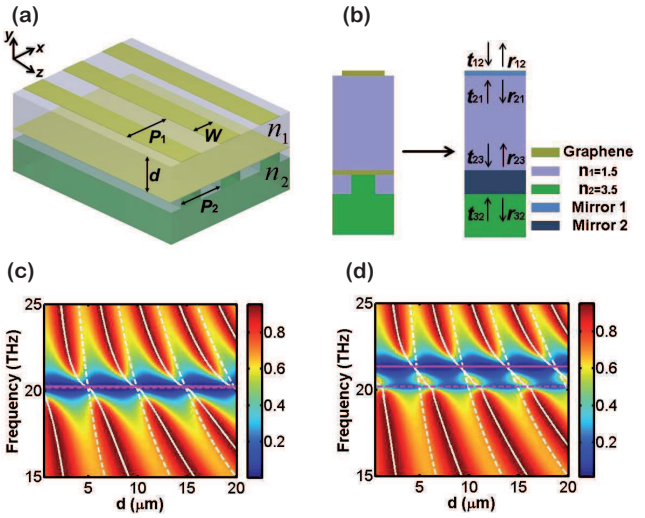

Fig. 4: (a) Schematic view of the far-field coupling system. The duty cycle and the depth of the grating is fixed to 0.5 and 300 nm, respectively. Note that the individual graphene ribbon in the upper periodic array is exactly on top of the corrugated part of the diffractive grating. (b) The entire system shown in panel (a) can be effectively described as a FP cavity with strongly dispersive resonant mirrors as long as the near-field coupling effect is negligible. (c) and (d): Simulated transmission contour plots at two different ribbon widths: (c) $W = 240\,\mathrm{nm}$; (d) $W = 228\,\mathrm{nm}$. Bare FP modes are presented as the white dashed lines, and the coupled modes computed from the semi-analytical model (Eq. 5) are depicted as white solid lines. Magenta solid and dashed horizontal lines represent the spectral positions of the bare LSPP and DSPP modes, respectively.

III. FAR-FIELD INTERFERENCE SCHEME (FFIS)

Using the NFCS as shown in Fig. 1, it is impossible to explore the far-field interaction between DSPPs and LSPPs. When the separation distance between the upper PAGR and the bottom graphene layer is well beyond the decay length of the evanescent diffraction orders, the DSPP mode, supported by the bottom graphene layer, cannot be excited at all. Thus, a newly proposed structure, that we suggest to term far-field interference scheme (FFIS) displayed in Fig. 4(a), is exploited to investigate the far-field interaction between DSPPs and LSPPs in graphene. It distinguishes from the NFCS in that a dielectric diffractive grating beneath the graphene layer causes the excitation of the DSPP mode as suggested in Ref. 12, even if the upper PAGR is far apart.

As displayed in Fig. 4(a), the upper PAGR, with array period P_1 and ribbon width W, and the lower graphene layer are separated by a dielectric spacer ($\varepsilon_1 = 2.25$) of thickness d. Here we use a silicon ($\varepsilon_2 = 12.25$) diffractive grating with grating period P_2 underneath the graphene layer to facilitate the excitation. For simplicity, we set

$P_1 = P_2 = P$. It is evident that in the FFIS near-field coupling between DSPP and LSPP modes is still present provided that the separation distance d is small enough. However, here a sufficiently large separation distance will be assumed in order to exclusively focus on the far-field interaction phenomenon between DSPPs and LSPPs. In passing we mention that the near-field effect in the FFIS resembles that in the NFCS.

Considering the transition to the far-field interference, as the structure dimension along the propagation direction of the incident wave is in the order of the wavelength, retardation effects have to be taken into account. In addition to that, pronounced Fabry-Perot (FP) modes can be supported in the system for large separation distances d. Thus, the FFIS can be effectively described as a FP cavity bounded with two strongly dispersive resonant mirrors as shown in Fig. 4(b). Since the extension of the two effective resonant mirrors along the wave propagation direction is extremely subwavelength, they can be regarded as metasurfaces. Therefore, the resonance condition characterizing the transmission maxima for the entire system reads

$$2n_1 d\frac{\omega}{c} + \varphi_1(\omega) + \varphi_2(\omega) = 2\pi M, \tag{5}$$

where c is the speed of light in vacuum, $n_1 = \sqrt{\varepsilon_1}$ is the refractive index of the spacer, M is a positive integer, $\varphi_1(\omega) = \arctan\left[\Im(r_{21})/\Re(r_{21})\right]$ and $\varphi_2(\omega) = \arctan\left[\Im(r_{23})/\Re(r_{23})\right]$ are the phase shifts upon reflection at the two effective resonant mirrors, respectively. The reflection/transmission coefficients indicated in Fig. 4(b), such as r_{21}, t_{21} and r_{23}, t_{23}, can be straightforwardly numerically calculated for either isolated mirror. Moreover, the transmission coefficient of the entire system for any specific larger separation distance d can be semi-analytically calculated using Airy's formula [38]

$$t = \frac{t_{12}t_{23}\exp(i\varphi)}{1 - r_{21}r_{23}\exp(i2\varphi)}, \tag{6}$$

where $\varphi = n_1 d(\omega/c)$.

Let us start the analysis with $P = 300\,\text{nm}$, and the identical Fermi energy $E_\text{F} = 600\,\text{meV}$ in upper PAGR and lower graphene layer. The simulated transmission spectra as a function of the spacer distance d for two different ribbon widths W are shown in Figs. 4(c) and (d). The spectral positions of the bare LSPP (ω_L) and DSPP (ω_D) modes are displayed by magenta solid and dashed lines, respectively, and the bare FP modes are shown as white dashed lines. It is evident that the semi-analytical formula (Eq. 5) accurately reproduces the resonance positions for larger separation distance d as shown by the white solid lines.

In Fig. 4(c) the width $W = 240\,\text{nm}$ is chosen such that $\omega_\text{L} \approx \omega_\text{D}$. In this scenario, the periodic transmittance pattern with transmission dips around the magenta solid/dashed line indicates the formation of hybrid LSPP-DSPP-FP modes. The spectral line width of the hybrid mode varies periodically, which can be attributed to the tailored spatial arrangement of the plasmonic modes (LSPP and DSPP modes). The spectral line width of the hybrid mode decreases drastically at definite spacer thicknesses where the Bragg criterion $d = N\pi n_1\omega_\text{L}/c$ is fulfilled [39].

A more interesting scenario occurs for $W = 228\,\text{nm}$ where $\omega_\text{L} \neq \omega_\text{D}$, as shown in Fig. 4(d). As a consequence of the spectrally detuned interactions between either the LSPP or the DSPP mode with the FP modes, a sequence of high transmittance spots arise between the magenta solid and dashed lines. They can be attributed to the fact that the FP modes are modulated by spectrally detuned LSPP and DSPP modes together. The transmission dips around the black solid (dashed) line are mainly induced by the formation of the hybrid LSPP-FP (DSPP-FP) modes. There is an obvious spectral distinction between these two kinds of transmission dips, as shown in Fig. 4(d), which is mainly due to the fact that the phase shift at the two effective mirrors is different.

IV. CONCLUSION

In this work we proposed two graphene based systems to facilitate the manipulation of the interaction between a localized surface plasmon polariton (LSPP) and a delocalized surface plasmon polariton (DSPP) in the near-field as well as in the far-field regime for the first time. In the near-field regime, both LSPP and DSPP modes can be regarded as particle-like plasmonic oscillators in the framework of plasmon hybridization theory. Therefore, by changing the geometrical parameters in the near-field coupling scheme (NFCS) and the Fermi energy of graphene, one can actually manipulate the physical properties of the individual oscillators. This allows to control the interaction between them as an entity. However, in the far-field regime, the radiative interaction mediated by the Fabry-Perot (FP) modes supported by the far-field interference scheme (FFIS) will be more pronounced. Thus, a picture of an effective FP cavity is proposed to provide an intuitive understanding for this interaction regime. Our findings may open up an avenue for the development of compact elements such as tunable sensors, switchers, and filters at IR and THz frequencies.

Acknowledgements

This work was supported by the German Federal Ministry of Education and Research (PhoNa) and by the Thuringian State Government (MeMa).

[1] K. S. Novoselov, A. K. Geim, S. Morozov, D. Jiang, Y. Zhang, S. Dubonos, I. Grigorieva, and A. Firsov, Science **306**, 666 (2004).

[2] A. K. Geim and K. S. Novoselov, Nature Materials **6**, 183 (2007).

[3] F. Bonaccorso, Z. Sun, T. Hasan, and A. Ferrari, Nature Photonics **4**, 611 (2010).

[4] A. Grigorenko, M. Polini, and K. Novoselov, Nature Photonics **6**, 749 (2012).

[5] P. Tassin, T. Koschny, and C. M. Soukoulis, Science **341**, 620 (2013).

[6] I. V. Iorsh, I. S. Mukhin, I. V. Shadrivov, P. A. Belov, and Y. S. Kivshar, Physical Review B **87**, 075416 (2013).

[7] R. Nair, P. Blake, A. Grigorenko, K. Novoselov, T. Booth, T. Stauber, N. Peres, and A. Geim, Science **320**, 1308 (2008).

[8] F. H. Koppens, D. E. Chang, and F. Garcia de Abajo, Nano Letters **11**, 3370 (2011).

[9] M. Jablan, H. Buljan, and M. Soljačić, Physical Review B **80**, 245435 (2009).

[10] A. Vakil and N. Engheta, Science **332**, 1291 (2011).

[11] J. Christensen, A. Manjavacas, S. Thongrattanasiri, F. H. Koppens, and F. Garcia de Abajo, ACS Nano **6**, 431 (2011).

[12] W. Gao, J. Shu, C. Qiu, and Q. Xu, ACS Nano **6**, 7806 (2012).

[13] A. Y. Nikitin, F. Guinea, F. J. Garcia-Vidal, and L. Martin-Moreno, Physical Review B **85**, 081405 (2012).

[14] M. Farhat, S. Guenneau, and H. Bağcı, Physical Review Letters **111**, 237404 (2013).

[15] P. Buslaev, I. Iorsh, I. Shadrivov, P. A. Belov, and Y. S. Kivshar, JETP Letters **97**, 535 (2013).

[16] R. Alaee, M. Farhat, C. Rockstuhl, and F. Lederer, Optics Express **20**, 28017 (2012).

[17] G. Pirruccio, L. MartiÂŽn Moreno, G. Lozano, and J. GoÂŽmez Rivas, ACS Nano **7**, 4810 (2013).

[18] S. Thongrattanasiri, F. H. Koppens, and F. J. G. de Abajo, Physical Review Letters **108**, 047401 (2012).

[19] Q. Bao, H. Zhang, B. Wang, Z. Ni, C. H. Y. X. Lim, Y. Wang, D. Y. Tang, and K. P. Loh, Nature Photonics **5**, 411 (2011).

[20] H. Cheng, S. Chen, P. Yu, J. Li, B. Xie, Z. Li, and J. Tian, Applied Physics Letters **103**, 223102 (2013).

[21] E. Carrasco, M. Tamagnone, and J. Perruisseau-Carrier, Applied Physics Letters **102**, 104103 (2013).

[22] P.-Y. Chen and A. Alù, ACS Nano **5**, 5855 (2011).

[23] P.-Y. Chen, J. Soric, Y. R. Padooru, H. M. Bernety, A. B. Yakovlev, and A. Alù, New Journal of Physics **15**, 123029 (2013).

[24] R. Filter, M. Farhat, M. Steglich, R. Alaee, C. Rockstuhl, and F. Lederer, Optics Express **21**, 3737 (2013).

[25] E. Prodan, C. Radloff, N. Halas, and P. Nordlander, Science **302**, 419 (2003).

[26] S. Zhang, D. A. Genov, Y. Wang, M. Liu, and X. Zhang, Physical Review Letters **101**, 47401 (2008).

[27] N. Liu, L. Langguth, T. Weiss, J. Kästel, M. Fleischhauer, T. Pfau, and H. Giessen, Nature Materials **8**, 758 (2009).

[28] F. Hao, Y. Sonnefraud, P. V. Dorpe, S. A. Maier, N. J. Halas, and P. Nordlander, Nano Letters **8**, 3983 (2008).

[29] R. F. Oulton, V. J. Sorger, D. Genov, D. Pile, and X. Zhang, Nature Photonics **2**, 496 (2008).

[30] V. Fedotov, M. Rose, S. Prosvirnin, N. Papasimakis, and N. Zheludev, Physical Review Letters **99**, 147401 (2007).

[31] H. Cheng, S. Chen, P. Yu, X. Duan, B. Xie, and J. Tian, Applied Physics Letters **103**, 203112 (2013).

[32] H. Iizuka and S. Fan, Applied Physics Letters **103**, 233107 (2013).

[33] A. Y. Nikitin, F. Guinea, F. J. García-Vidal, and L. Martín-Moreno, Physical Review B **84**, 161407 (2011).

[34] A. Christ, T. Zentgraf, S. Tikhodeev, N. Gippius, J. Kuhl, and H. Giessen, Physical Review B **74**, 155435 (2006).

[35] L. Ju, B. Geng, J. Horng, C. Girit, M. Martin, Z. Hao, H. A. Bechtel, X. Liang, A. Zettl, Y. R. Shen, et al., Nature Nanotechnology **6**, 630 (2011).

[36] A. Salomon, R. J. Gordon, Y. Prior, T. Seideman, and M. Sukharev, Physical Review Letters **109**, 073002 (2012).

[37] V. Agranovich, M. Litinskaia, and D. Lidzey, Physical Review B **67**, 085311 (2003).

[38] M. C. Teich and B. Saleh, Canada, Wiley Interscience p. 3 (1991).

[39] R. Taubert, R. Ameling, T. Weiss, A. Christ, and H. Giessen, Nano Letters **11**, 4421 (2011).